Study and Comparison of several Permanent-Magnet excited Rotor Types regarding their Applicability in Electric Vehicles

Thomas Finken, Marco Hombitzer and Kay Hameyer
Institute of Electrical Machines
RWTH Aachen University
Schinkelstr. 4, 52056 Aachen, Germany
Email: thomas.finken@iem.rwth-aachen.de

***Abstract*—Due to the limited available space and the high demands in power density and overall efficiency, the permanent magnet synchronous machine (PMSM) is the mainly applied machine type in parallel hybrid electric vehicles (HEV). This machine is used as well in many full electric vehicles (EV). In this work, several permanent-magnet excited rotor types are studied regarding their applicability in EVs and HEVs, and are compared in terms of among others: their maximum torque and power, power density, their efficiency map, field-weakening capability, overload capacity and torque ripple.**

I. Introduction

An increasing ecological awareness and the shortage of fossil-fuel resources are strong incentives to develop more efficient vehicles, with lower fuel consumption but without reducing driving comfort. The hybrid electric vehicle (HEV), which combines the drive power of an internal combustion engine and that of one or several electrical machines, and the full electric vehicle (EV) are promising concepts in this regard. According to the considered vehicle concept, the electrical machine has to be as efficient as possible at various operating points. Besides the fast start/stop function, it can also operate as a generator, as support traction in the so called boost operation, as a drive during electrical traction, as well as electrodynamic brake for recuperation. With such a functionality and the requirements in power, efficiency, installation space and weight, the design of the machines is particularly challenging.

Due to the limited available space and the high demands in power density and overall efficiency, the permanent magnet synchronous machine (PMSM) is the most suitable and the mainly applied machine type in parallel HEVs [1]- [5]. If the main requirement is to save weight and space, combined with a good efficiency at low speeds, this machine type is applied in EVs as well - especially in wheel-hub motors (in-wheel motors). In this work several permanent-magnet excited rotor types are studied regarding their applicability in EVs and HEVs. They are compared in terms of (among others): their maximum torque and power, power density, efficiency map, field-weakening capability, overload capacity and their torque ripple.

II. Studied rotor types

The rotor types under study, depicted in Fig. 1, are: a rotor with surface mounted magnets (SM-PMSM), a rotor with inset surface magnets (SI-PMSM), with internal (buried) magnets (I-PMSM), with v-shaped internal magnets (VI-PMSM) and a rotor with radial arranged internal magnets (RI-PMSM).

The electrical machine design is conducted under the constraint that the outer dimensions of the machine are fixed. The degrees of freedom are the rotor diameter, the pole-pair number and the type of winding (i.e. concentrated or distributed winding). In order to study the effect of the pole-pair number and the winding type, the machine types are designed for two pole-pair numbers ($p = 4$ and $p = 8$) and two different winding types (concentrated winding and a distributed winding with a distribution factor (slot/pole ratio) of $q = 2$). For each winding type and pole pair number, the optimum rotor radius is determined regarding the available maximum torque. All rotor configurations consider mechanical stress calculations to assure a sufficient mechanical strength at high speeds.

The first degree of freedom is the rotor diameter D, whereas

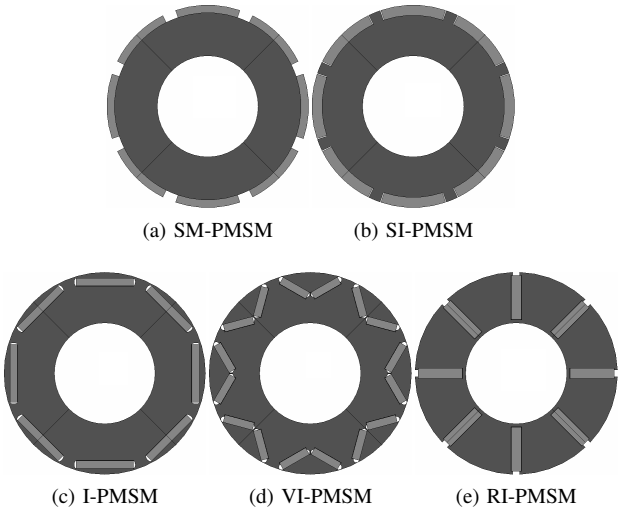

(a) SM-PMSM (b) SI-PMSM (c) I-PMSM (d) VI-PMSM (e) RI-PMSM

Fig. 1: Studied permanent-magnet excited rotor types.

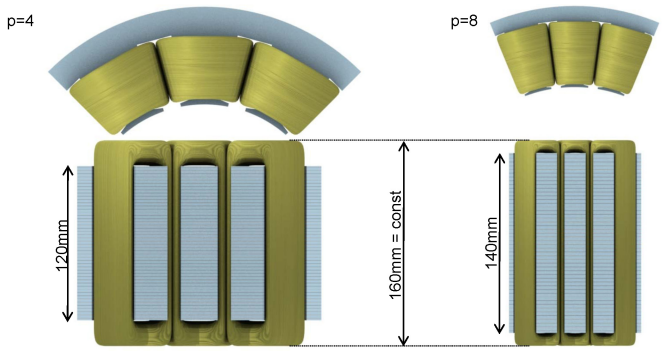

(a) Concentrated winding

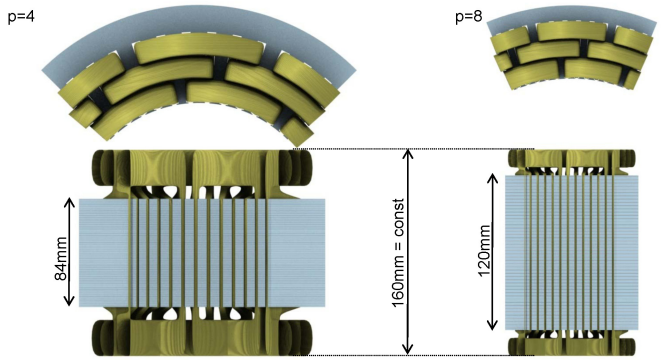

(b) Distributed winding (q=2)

Fig. 2: The active length depending on p.

the stator diameter D_S remains constant. A given air gap force produces a torque proportional to the radius, i.e. the torque is at least linearly proportional to the diameter. Moreover, if the diameter increases, there is more space for magnets around the rotor which increases the specific magnetic loading. Therefore, torque and power increase with the diameter. But increasing the rotor diameter lowers the volume of the stator. The area available for stator coils decreases then, and if a constant current density is assumed, the specific electric loading A decreases as well. As a result, a maximum of the torque can be expected for an intermediate value of the rotor diameter D.

The pole-pair number p influences the rotor size and thus the volume of a machine when using analytical formulas - increasing the poles increases the force generated by the motor. Furthermore, the stator-yoke height and the length of the end winding take up less space as the pole pair number increases, so that the active length of the motor can reach the fixed total length (see Fig. 2). Thus, the power density increases with increasing power at constant volume. But increasing the number of poles implies decreasing the magnet width and increasing the amount of magnet leakage flux. The force will therefore not increase indefinitely. Moreover, iron losses increase more than linearly with the frequency of the stator currents and of the alternating magnetic field, which is proportional to the pole pair number. Iron losses are the dominant losses in PMSMs at high rotational speeds. So the total losses increase significantly with increasing pole number at high speed whereas the overall efficiency decreases.

Both winding types considered in this study have their own advantages and disadvantages [6]- [8]. Concentrated windings reduce the dimensions of the coil ends and improves the active length of the machine, so that the power density is higher than that of machines with distributed windings. In addition, Ohmic losses related to the output power are reduced, because end windings do not contribute to the torque generation but generate thermal heat by copper losses. Moreover, concentrated windings significantly increase the copper fill factor (up to $f_{cu} = 70\%$) and are better suited for automated manufacturing, because rectangular conductors, preformed coils and segmented cores are possible to apply. However, concentrated windings suffer from increased slotting effect (alternating magnetic reluctance) and significantly increased rotor losses, i.e. the magnet's eddy-current losses in particular.

Distributed windings feature better winding factors than concentrated windings, so that machines with distributed windings require a smaller number of turns, but its end windings take up more space and the winding volume increases. Furthermore, the copper fill factor is smaller (up to $f_{cu} = 50\%$), as this winding type has to be produced as moved-in winding. Therefore, the application of distributed windings increase the Ohmic losses. The main advantage of the distributed winding is the possibility to vary the slot/pole ratio (zoning) and to apply short-pitching. By zoning (spreading a coil onto multiple slots q) and short-pitching (displacement of single or several turns into slots nearby), particular harmonics of the magnetic field can be weakened. Finally, distributed windings reduce the slotting effect and consequently the rotor losses, because the iron losses, depending on the field harmonics, and the magnet's eddy-current losses, depending on the slotting effect, are lower than that of machines with concentrated windings.

III. Numerical Calculation Methods

Saturation- and flux-leakage effects cannot be determined accurately by analytical formulas. Quasi-static numerical FE simulations are hence performed for each geometry. All simulations were conducted with the in-house FEM software *iMOOSE* [9].

First, a ***No-Load Simulation*** is performed to calculate the stator flux-linkage and the back-emf. In addition, the magnetic flux distribution is visualized.

To determine the overload capability, a ***Demagnetization Test*** is conducted. The worst case would be a fault in the power electronics and control, feeding the maximum current into negative direct axis ($I_d = -I_{max}$). The demagnetization of the permanent magnets, which is maximum then, should not cause irreversible demagnetization. In order to determine this limit, a current is fed in negative direct axis and the current density is stepwise increased to determine the maximum current I_{max}, still having the working point on the linear part of the demagnetization characteristic.

The torque of a PMSM can be determined by:

$$T = \frac{3p}{\omega} \cdot [U_p - I_d \cdot (X_q - X_d)] \cdot I_q. \tag{1}$$

Table I: Data of CW geometries.

	SM-PMSM		SI-PMSM		I-PMSM		VI-PMSM		RI-PMSM	
	p=4	p=8	p=4	p=8	p=4	p=8	p=4	p=8	p=4	p=8
stator diameter (mm)	270	270	270	270	270	270	270	270	270	270
rotor diameter (mm)	75	85	75	85	75	85	80	90	85	85
total length (mm)	160	160	160	160	160	160	160	160	160	160
active magnetic length (mm)	120	140	120	140	120	140	120	140	120	140
active volume (dm^3)	9.2	9.2	9.2	9.2	9.2	9.2	9.2	9.2	9.2	9.2
max. overload current (I / I$_n$)	2	4.5	1.5	3.5	2	5	2	5	2	5
rated speed (min^{-1})	2000	2000	2000	2000	2000	2000	2000	2000	2000	2000
rated torque T_n (Nm)	210	254	221	261	216	242	216	221	199	325
max. torque T_{max} (Nm)	398	662	325	680	387	598	386	557	316	616
rated power P_n (kW)	44	53	46	55	45	51	45	46	42	68
overload power P_{max} (kW)	83	139	68	142	81	125	81	117	66	129
rated power density (kW/dm^3)	4.8	5.8	5.0	5.9	4.9	5.5	4.9	5.0	4.5	7.4
overload power density (kW/dm^3)	9.1	15.1	7.4	15.5	8.8	13.6	8.8	12.7	7.2	14.0
number of turns	27	10	25	10	23	10	21	10	20	9
inductance L_d (mH)	2.92	0.82	2.57	0.82	2.64	1.03	2.57	1.10	3.42	0.58
inductance L_q (mH)	2.97	0.84	4.48	1.35	5.08	1.69	5.37	2.09	5.58	0.89
max. field weakening n_{max}/n_n	2.95	1.90	3.00	2.15	3.00	3.00	3.00	3.00	3.00	1.70
surface-loss density $P_{v\,ges,n}/A$ (W/dm^2)	373	460	387	555	243	326	145	188	128	255
surface-loss density $P_{v\,ges,0}/A$ (W/dm^2)	1503	2059	1507	2053	237	498	232	378	303	1024
magnet mass (kg)	2.0	2.6	2.0	2.6	1.9	2.6	2.0	2.5	1.8	4.2
magnet utilization, P_n/m_{PM} (Nm/kg)	22.2	20.1	23.4	20.7	24.0	19.3	23.2	18.3	23.0	16.0
magnet utilization, P_{max}/m_{PM} (Nm/kg)	42.1	52.4	34.4	53.8	43.0	47.8	41.4	46.2	36.4	30.4
max efficiency	90.8%	92.5%	91.7%	91.8%	93.5%	93.5%	95.9%	95.5%	95.8%	95.4%

Table II: Data of DW geometries.

	SM-PMSM		SI-PMSM		I-PMSM		VI-PMSM		RI-PMSM	
	p=4	p=8	p=4	p=8	p=4	p=8	p=4	p=8	p=4	p=8
stator diameter (mm)	270	270	270	270	270	270	270	270	270	270
rotor diameter (mm)	75	85	75	85	75	90	80	90	85	90
total length (mm)	160	160	160	160	160	160	160	160	160	160
active magnetic length (mm)	84	120	84	120	84	120	84	120	84	120
active volume (dm^3)	9.2	9.2	9.2	9.2	9.2	9.2	9.2	9.2	9.2	9.2
max. overload current (I / I$_n$)	2	5	2	5	2.5	5	3	5	2	5
rated speed (min^{-1})	2000	2000	2000	2000	2000	2000	2000	2000	2000	2000
rated torque T_n (Nm)	175	207	183	213	174	188	171	174	148	234
max. torque T_{max} (Nm)	319	505	332	518	307	484	399	437	237	463
rated power P_n (kW)	37	43	38	45	36	39	36	36	31	49
overload power P_{max} (kW)	67	106	69	108	64	101	84	92	50	97
rated power density (kW/dm^3)	4	4.7	4.2	4.8	4	4.3	3.9	4	3.4	5.3
overload power density (kW/dm^3)	7.3	11.5	7.6	11.8	7	11	9.1	10	5.4	10.5
number of turns	34	11	31	11	29	11	27	12	29	9
inductance L_d(mH)	3.07	0.62	2.49	0.58	2.74	0.71	2.51	0.93	4.34	0.41
inductance L_q (mH)	3.46	0.71	5.19	1.22	6.28	1.67	6.58	2.21	7.06	0.62
max. field weakening n_{max}/n_n	2.35	1.50	2.70	1.60	3.00	1.75	3.00	2.50	3.00	1.35
surface-loss density $P_{v\,ges,n}/A$ (W/dm^2)	234	287	235	306	176	219	155	210	136	269
surface-loss density $P_{v\,ges,0}/A$ (W/dm^2)	635	949	642	938	191	506	193	404	270	1132
magnet mass (kg)	1.4	2.3	1.4	2.3	1.3	2.4	1.4	2.2	1.3	3.9
magnet utilization, P_n/m_{PM} (Nm/kg)	26.4	19.1	27.6	19.7	27.6	16.5	26.2	16.8	24.4	12.7
magnet utilization, P_{max}/m_{PM} (Nm/kg)	48.1	46.6	50	47.8	48.8	42.4	61.1	42.3	39	25.1
max efficiency	91.9%	93.8%	92.4%	93.6%	95.0%	95.0%	95.5%	94.8%	94.8%	94.6%

It consists of the synchronous torque T_{syn} and, if $X_q \neq X_d$, the reluctance torque T_{rel}:

$$T = \underbrace{\frac{3p}{\omega} \cdot U_p I_q}_{T_{syn}} \underbrace{- \frac{3p}{\omega} \cdot I_q I_d \cdot (X_q - X_d)}_{T_{rel}}. \tag{2}$$

With $I_q = I \cos\psi$, $I_d = I \sin\psi$ and the field-weakening angle ψ, the torque can be written as:

$$T = \hat{T}_{syn} \cos(\psi) - \hat{T}_{rel} \sin(2\psi). \tag{3}$$

This means the torque depending on the field-weakening angle consists of a fundamental ($\hat{T}_{syn}$) and the first harmonic ($\hat{T}_{rel}$). The field-weakening angle ψ, at which the sum of the synchronous torque and the reluctance torque (and thus the available total torque) is maximum, is called the optimum field-weakening angle ψ_{opt}.

The so called ***"Locked-Rotor Test"*** allows now determining the absolute value of the synchronous torque $\hat{T}_{syn}$, the absolute value of the reluctance torque $\hat{T}_{rel}$, the optimum field-weakening angle ψ_{opt} and the resulting maximum torque. This calculation is performed for a stepwise increasing stator-current density in order to determine how those quantities depend on the load current.

The direct- and quadrature-axis inductances (L_d and L_q) are calculated by means of the L_dL_q***-Computation*** as a function of the load current and the field weakening angle

ψ. The inductances L_d and L_q determine the field weakening capability, as well as the torque for each operation point by (1). For this reason, they are required for the machine's control, especially in the range of field weakening.

In order to minimize fuel consumption, the efficiency of the drive must be carefully optimized and, therefore, all losses need be accurately evaluated for all operation points. This computation is called the ***Operation Point Simulation***. At this step, the optimum field-weakening angle ψ_{opt} is used to set the maximum torque over the base speed range, whereas ψ is set by means of control strategies in the field weakening range.

Ohmic losses are estimated taking end windings into account. Iron losses are computed by means of quasi-static numerical FE simulations and an improved post-processing formula based on the loss-separation principle [10]- [11], and that considers rotational hysteresis losses as well [12]. The eddy-current density in the permanent magnets is calculated by means of a transient 3D-FE approach, as described in [13]- [14]. The eddy-current density and the specific conductivity of the magnet material are used to determine the eddy-current losses by integration over the magnet's volume. All eddy-current losses are calculated with an axial magnet segmentation of 4 segments.

On basis of this loss calculation it is possible to determine the total losses for all operation points (i.e. as a function of speed and torque). Resulting from the total losses and the output power, the efficiency can be calculated. The results are depicted in two-dimensional maps: the loss maps and efficiency maps.

Furthermore, the ***Operation Point Simulation*** calculates the $T(t)$-characteristics and with that, by means of a FFT, the torque's harmonic content - the torque ripple.

IV. Results of Numerical Calculations

The geometrical data resulting from the design process are listed in Table I for the concentrated winding and in Table II for the distributed winding machines.

In Fig. 3, the efficiency maps are depicted for all variations of the I-PMSM geometry. The line of rated torque (dashed line) is determined by assuming that the rated torque is limited by the rated current density (here 6A/mm^2) up to the rated speed. From the point of rated speed and rated torque on, the torque curve declines over speed, keeping the output power constant. The maximum torque (full line) results from the maximum torque determined by the demagnetization test. This maximum current is kept until base speed, above base speed the output power remains constant.

As described, the application of the concentrated winding decreases the Ohmic losses and increases the eddy-current losses of the machine. Since the Ohmic losses, which remain constant with speed, are the main losses at lower speeds and the eddy-current losses, which increase with f^2, are the main losses at higher speeds, the application of the concentrated winding shifts the range of best efficiency to lower speeds.

The application of the distributed winding shifts the range of best efficiency to higher speeds, for it increases the Ohmic losses and decreases the eddy-current losses of the machine. Increasing the pole-pair number stretch the map towards a higher torque, so higher power densities are possible. However, it has to be considered that the efficiency at lower torques decreases, because the decay to $\eta(T = 0\,\mathrm{Nm}) = 0$ is stretched, too. So an increase of the power density by raising the pole number makes no sense if the machine would be oversized and the most frequent operation points would be located below the range of best efficiency then.

In Fig. 4 the loss maps, and in Fig. 5 the resulting efficiency maps are depicted for all rotor types, the maps are depicted exemplary for geometries with concentrated winding and a pole-pair number of $p = 8$. The total losses per outer stator surface are used for a first estimation of the required cooling effort or the thermal limits of the machine. These surface-loss density is determined for two operation points and listed in Table I and Table II. The first point is the nominal point with the speed $n = 2000\,\mathrm{min}^{-1}$ and the torque $T = T_n$, the second at maximum speed ($n = 6000\,\mathrm{min}^{-1}$) and no-load ($T = 0\,\mathrm{Nm}$).

Since the magnets are not protected from the stator field reaction and slotting effects, high eddy-current losses occur in the geometries with surface mounted or inset magnets (SM-PMSM and SI-PMSM). These losses are the main losses at high speed range, therefore the SM-PMSM and the SI-PMSM provide very low efficiencies at high speeds. Advantage of these geometries is the high overload torque offered.

In geometries with internal or buried magnets, the magnets are protected from the stator field reaction and slotting effects. Thus the eddy-current losses are smaller, and the efficiency at high speed is higher. The VI-PMSM and the RI-PMSM provide the highest maximum efficiency and the widest speed

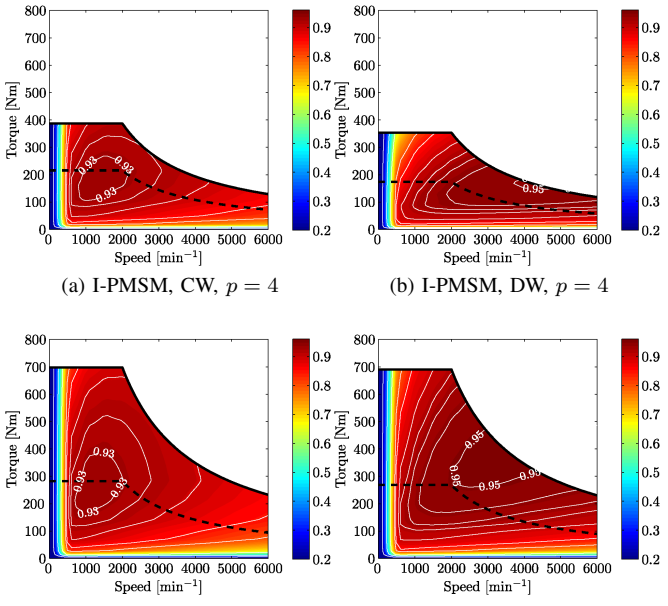

(a) I-PMSM, CW, $p = 4$ (b) I-PMSM, DW, $p = 4$

(c) I-PMSM, CW, $p = 8$ (d) I-PMSM, DW, $p = 8$

Fig. 3: The efficiency maps of the I-PMSM geometry.

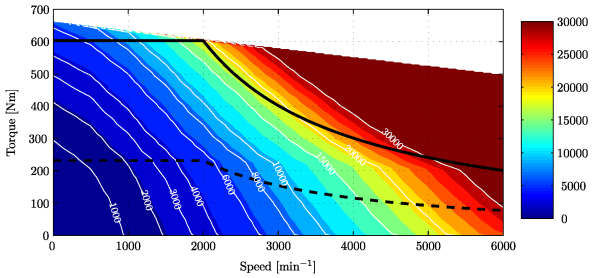

(a) SM-PMSM, CW

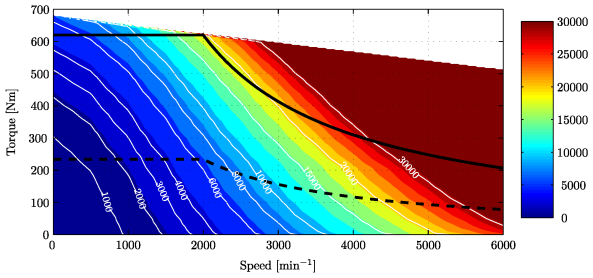

(b) SI-PMSM, CW

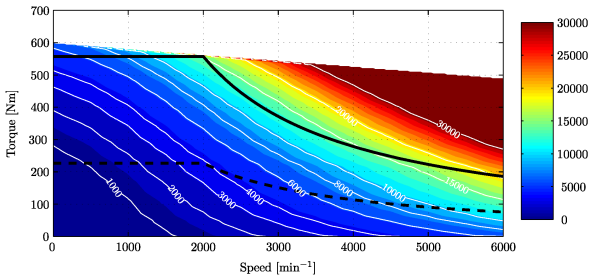

(c) I-PMSM, CW

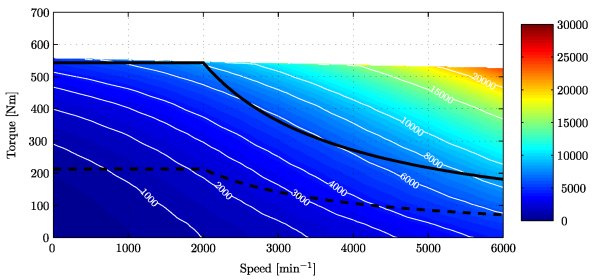

(d) VI-PMSM, CW

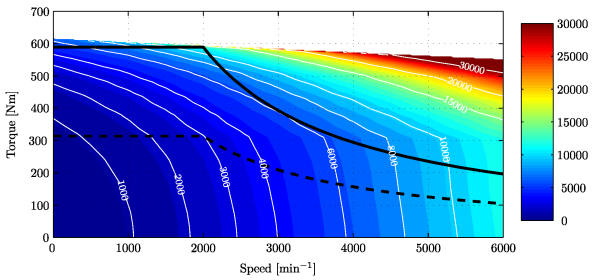

(e) RI-PMSM, CW

Fig. 4: The total loss maps in Watt (W) ($p = 8$).

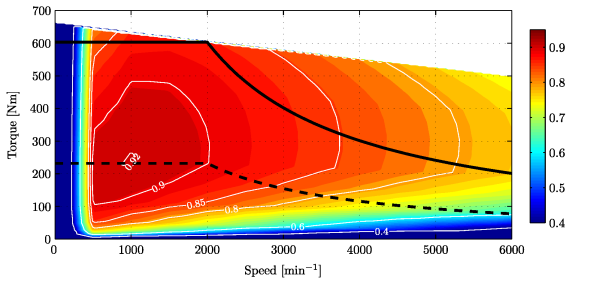

(a) SM-PMSM, CW

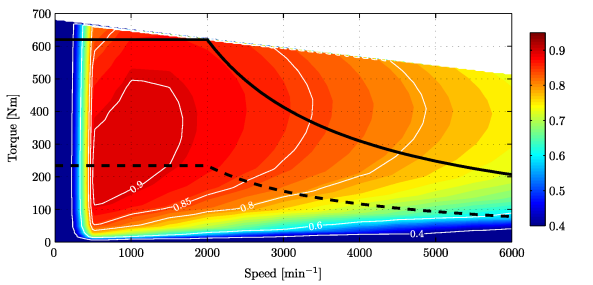

(b) SI-PMSM, CW

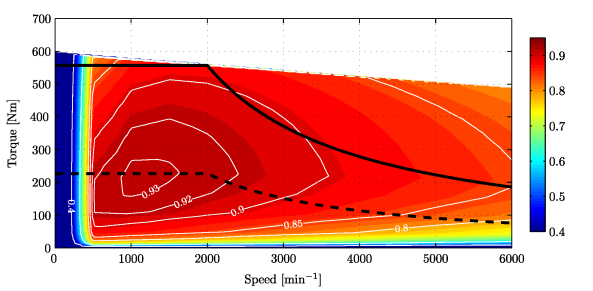

(c) I-PMSM, CW

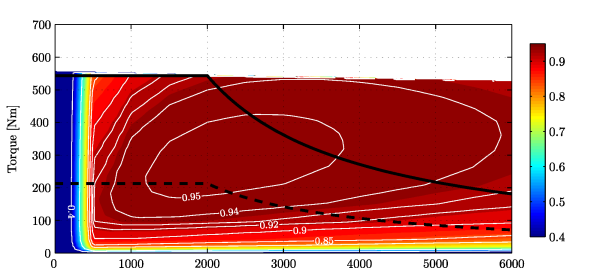

(d) VI-PMSM, CW

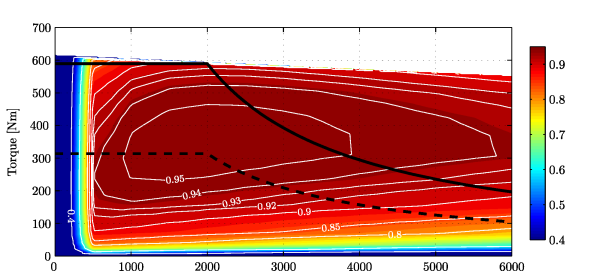

(e) RI-PMSM, CW

Fig. 5: The efficiency maps ($p = 8$).

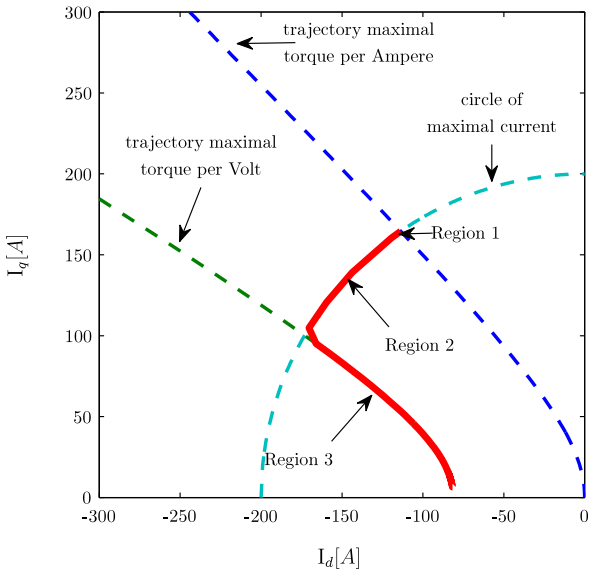

Fig. 6: PMSM operation points in the I_d-I_q coordinate system.

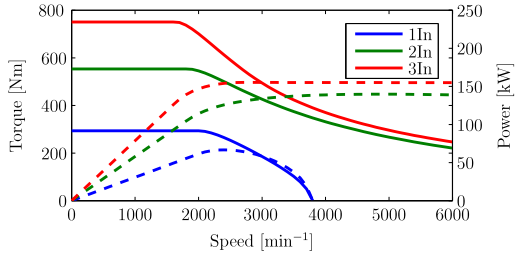

(a) $T(n)$ and $P(n)$ of SM-PMSM, CW, $p = 8$

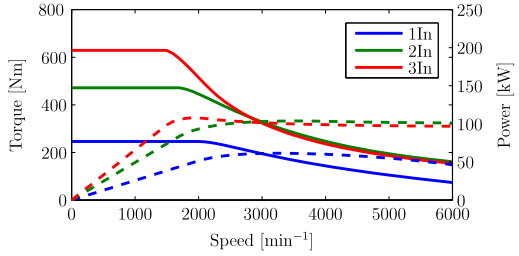

(b) $T(n)$ and $P(n)$ of VI-PMSM, CW, $p = 8$

Fig. 7: $T(n)$- and $P(n)$- characteristics.

and torque range in which the efficiency is good ($\eta > 0.90$). With regard to the overall efficiency and the vehicle's energy consumption the VI-PMSM and the RI-PMSM would be the most suitable rotor types. A disadvantage of the RI-PMSM is the linearly increasing magnet material volume by increasing the pole number. As a result the magnet utilization of the RI-PMSM geometry decreases with increasing pole number. The magnet utilization (torque per magnet mass) is determined for all geometries and rotor variations depending on load current, first for nominal current and second for maximum overload current to take possible saturation effects into account. The best magnet utilization, and thus the best cost-benefit ratio with respect to the magnets, is offered by geometries with surface mounted magnets (SM-PMSM and SI-PMSM) or with v-shaped internal magnets (VI-PMSM).

To determine the field-weakening capability of all geometries, the torque- and power-versus speed characteristics are determined by means of maximum-torque-per-ampere (MTPA) and maximum-torque-per-flux (MTPF) control, see Fig. 6. For operation points in the base speed range (Region 1) the phase voltage is below the maximum voltage, which in turn is limited by the dc-link voltage of the power converter, so that the phase current is constrained by the magnet demagnetization limit and further thermal limitations or the power electronics' maximal current. In that speed range, the maximum torque T_{max} per current (MTPA-control) is achieved with the optimum field-weakening angle ψ_{opt}. For operation points in the field weakening range, the control strategy of the power converter keeps the phase voltage to its maximum by increasing ψ (Region 2, in Fig. 6). In some cases, according to the quantities L_d and L_q (and therefore depending on the geometry), there exists an operation point within the field weakening range, where a further increase of the rotor speed n requires to reduce the current below its maximum. From here on (Region 3, in Fig. 6), the power controller follows the maximum torque per voltage curve (MTPV-control). Assuming a nominal speed of $n_n = 2000\,\mathrm{min}^{-1}$ and a maximum phase voltage of U_{ph} =280 V, this results in the characteristics exemplary depicted in Fig. 7a and Fig. 7b.

To ensure a good comparability, all geometry variations are optimized with respect to the torque ripple by means of a pole-arc variation, i.e. the pole-arc ratio resulting in a minimum torque ripple was determined for each geometry.

In Table III and Table IV all geometries are evaluated and compared. The range of values for each criterion and pole-pair number is divided into five subranges of equal widths, labeled "++" for the upper subrange (best performance) and "−−" for the lowest subrange (worst performance). When evaluating the magnet mass it is considered that the lowest subrange instead of the highest one is the optimum. Since the outer dimension is fixed and remains constant for all geometries, the evaluation of power and power density is equal to the torque, thus they are not tabulated.

Examining the evaluation of all geometries with $p = 4$, the geometry with v-shaped internal magnets (VI-PMSM) scores best. The VI-PMSM geometry is close, both clearly in front of the other geometries (especially with distributed windings). For high pole-pair numbers the RI-PMSM scores worst, mainly due to its bad magnet utilization.

To decide which geometry at which pole-pair number is best, the evaluation criteria has to be weighted. Therefore, the geometry with most positive evaluations is not necessarily the best and most suitable for a specific vehicle. As a result, the weighting factor for each property has to be defined depending on vehicle concept and intended purpose.

V. Conclusion

In this work several permanent-magnet excited rotor types are designed and compared in terms of their maximum torque

Table III: rating of geometries, $p = 4$

	SM-PMSM		SI-PMSM		I-PMSM		VI-PMSM		RI-PMSM	
	CW	DW	CW	DW	CW	DW	CW	DW	CW	DW
max. overload (I_{max}/I_n)	o	o	−−	o	o	+	o	++	o	o
nominal torque M_n (Nm)	++	o	++	o	++	o	++	o	+	−−
max. torque M_{max} (Nm)	++	+	−	+	++	+	++	++	o	−−
magnet mass m_{PM} (kg)	−−	+	−−	+	−−	+	−−	+	−−	++
magnet utilization, P_n/m_{PM} (Nm/kg)	−−	++	−	++	o	++	−	+	−	o
magnet utilization, P_{max}/m_{PM} (Nm/kg)	o	+	−−	+	o	++	o	++	−	o
max. field weakening, n_{max}/n_e	+	−−	++	o	++	++	++	++	++	++
torque ripple	+	+	o	−−	+	+	+	++	−	−−
surface-loss density , $Pv_{ges,0}/A_{stat}$ (W/dm^2)	−−	o	−−	o	+	++	+	+	+	+
surface-loss density $Pv_{ges,n}/A_{stat}$ (W/dm^2)	−−	o	−−	o	o	+	+	+	++	+
max. efficiency	−−	−	−	−	o	++	++	++	++	++

Table IV: rating of geometries, $p = 8$.

	SM-PMSM		SI-PMSM		I-PMSM		VI-PMSM		RI-PMSM	
	CW	DW	CW	DW	CW	DW	CW	DW	CW	DW
max. overload (I_{max}/I_n)	+	++	−−	++	++	++	++	++	++	++
nominal torque M_n (Nm)	o	o	o	o	o	−	−	−−	++	+
max. torque M_{max} (Nm)	++	+	++	+	o	o	−	−−	+	−
magnet mass m_{PM} (kg)	+	+	+	+	+	+	+	++	−−	−−
magnet utilization, P_n/m_{PM} (Nm/kg)	+	++	+	++	o	+	o	+	−	−−
magnet utilization, P_{max}/m_{PM} (Nm/kg)	++	++	++	++	+	++	+	++	−−	−
max. field weakening, n_{max}/n_e	o	−−	o	−	++	−	++	+	−	−−
torque ripple	o	++	−	−−	−	−	o	+	−	−−
surface-loss density $Pv_{ges,0}/A_{stat}$ (W/dm^2)	−−	o	−−	o	+	+	++	+	o	o
surface-loss density $Pv_{ges,n}/A_{stat}$ (W/dm^2)	−	o	−−	o	o	+	++	+	+	+
max. efficiency	−	+	−−	+	o	++	++	++	++	++

and power, power density, their loss- and efficiency-maps, field-weakening capability, overload capacity and torque ripple. The different machine type's performances are compared to each other in a synoptic table. That offers an overview and helps to chose the most suitable geometry depending on the vehicle concept and its particular specifications in EV-Traction.

REFERENCES

[1] M. Zeraoulia, M.E.H. Benbouzid, D. Diallo. "Electric Motor Drive Selection Issues for HEV Propulsion Systems: A Comparative Study", *IEEE Trans. on Vehicular Technology*, Vol.55, No.6, November 2006.

[2] M. Yabumoto, C. Kaido, T. Wakisaka, T. Kubota, N. Suzuki. "Electrical Steel Sheet for Traction Motors of Hybrid/Electrical Vehicles", *Nippon Steel Technical Report*, No.87, July 2003.

[3] J.G.W. West. "Propulsion systems for hybrid electric vehicles", *Electrical Machine Design for Electric and Hybrid-Electric Vehicles, IEE Colloquium on*, pp. 1/1 - 1/9, October 1999.

[4] C.C. Chan. "An overview of electric vehicle technology", *Proceedings of the IEEE*, Volume 81, Issue 9, Page(s):1202 - 1213, September 1993.

[5] Thomas Finken, Matthias Felden, Kay Hameyer. "Comparison and design of different electrical machine types regarding their applicability in hybrid electrical vehicles", *Proceedings of the ICEM*, September 2008.

[6] J. Cros, P. Viarouge, "Synthesis of high performance PM motors with concentrated windings.", *IEEE Transaction on Energy Conversion,* Vol. 17, Issue 2, p. 248-253, June 2002.

[7] B. Stumberger, G. Stumberger, M. Hadziselimovic, I. Zagradisnik, A. Hamler, M. Trlep, "Permanent magnet synchronous motor with exterior-rotor: Distributed or concentrated windings - motor performance comparison.", *COMPEL - The International Journal for Computation and Mathematics in Electrical and Electronic Engineering,* Vol. 25, Issue 3, p. 721 - 726, 2006.

[8] K. Yamazaki, Y. Fukushima, M. Sato, "Loss Analysis of Permanent-Magnet Motors With Concentrated Windings-Variation of Magnet Eddy-Current Loss Due to Stator and Rotor Shapes.", *IEEE Transactions on Industry Applications,* Vol. 45, Issue 4, p. 1334-1342, July 2009.

[9] Institute of Electrical Machines, RWTH Aachen University. "In-house FE package iMOOSE." Internet: http://www.iem.rwth-aachen.de/index.pl/simulatio__design, 2009 [Jan. 28, 2010].

[10] G. Bertotti, "General properties of power losses in soft ferromagnetic materials.", *IEEE Transactions on Magnetics,* Vol. 24, No. 1 p. 621-630, January 1988.

[11] G. Bertotti, A. Boglietti, M. Chiampi, D. Chiarabaglio, F. Fiorillo, M. Lazzari, "An improved estimation of iron losses in rotating electrical machines.", *IEEE Transactions on Magnetics,* Vol. 27, No. 6, p. 5007-5009, November 1991.

[12] S. Jacobs, D. Hectors, F. Henrotte, M. Hafner, M. H. Gracia, K. Hameyer, P. Goes, "Magnetic material optimization for hybrid vehicle PMSM drives.", *World Electric Vehicle Journal,* online: www.evs24.org/wevajournal, Vol. 3, May 2009.

[13] C. Kaehler, G. Henneberger, "An Eddy-current computation in the claws of synchronous a claw-pole alternator in generator mode.", *IEEE Transactions on Magnetics,* Vol. 38, No. 2, p. 1201-1204, March 2002.

[14] C. Kaehler, G. Henneberger, "Eddy-current computation on a one pole-pitch model of a synchronous claw-pole alternator.", *COMPEL - The International Journal for Computation and Mathematics in Electrical and Electronic Engineering,* v 22, n 4, p 834-846, 2003.